SCIENTIFIC REP⚙RTS

OPEN

Structure-property relationship of Co$_2$MnSi thin films in response to He^{+}-irradiation

Franziska Hammerath[1], Rantej Bali[2], René Hübner[2], Mira R. D. Brandt[1], Steven Rodan[1], Kay Potzger[2], Roman Böttger[2], Yuya Sakuraba[3] & Sabine Wurmehl[1,4]

We investigated the structure-property relationship of Co$_2$MnSi Heusler thin films upon the irradiation with He^{+} ions. The variation of the crystal structure with increasing ion fluence has been probed using nuclear magnetic resonance (NMR) and transmission electron microscopy (TEM), and associated with the corresponding changes of the magnetic behavior. A decrease of both the structural order and the moment in saturation is observed. Specifically, we detect a direct transition from a highly $L2_1$-ordered to a fully $A2$-disordered structure type and quantify the evolution of the $A2$ structural contribution as a function of ion fluence. Complementary TEM analysis reveals a spatially-resolved distribution of the $L2_1$ and $A2$ phases showing that the $A2$ disorder starts at the upper part of the films. The structural degradation in turn leads to a decreasing magnetic moment in saturation in response to the increasing fluence.

Highly $L2_1$-ordered Heusler compounds (X$_2$YZ) are promising candidates for half-metallic ferromagnetism[1–6] whose 100% spin polarization gives rise to interesting applications in spintronic devices, such as magnetic tunnel junctions (MTJ) or giant magnetoresistance (GMR) devices[7–11]. In combination with its high Curie temperature (985 K), saturation moment (5 μ_B) and large band gap for the minority spin states (0.4–0.8 eV)[2,8,9,12,13], Co$_2$MnSi is especially well-suited for such applications. Chemical order has strong impact on the properties in general. This relationship is in particular important for half-metallic ferromagnetic materials, since their spin polarisation is downgraded rapidly for certain types of disorder[14–17]. As a consequence, the performance of any application based on the spin polarisation, e.g. GMR devices, will in turn strongly depend on the degree of chemical order of the material[18]. Hence, a control of the structure-property relationship is a crucial factor for their use in high-end applications. The classical route to address and control the structural order and, thus, the properties of such highly functional materials is post-growth annealing, where the annealing temperature and/or annealing time have to be optimized.

Another route to control the structure and magnetic properties of functional materials is the irradiation with light ions, which is known to strongly modify their magnetic properties[19–22]. Studies on Co$_2$MnSi thin films reported improved structural properties upon the irradiation with He^{+} ions within a certain range of fluences (1×10^{14}–5×10^{14} ions/cm^2, 30 keV), going along with an improvement of the electronic and magnetic properties[23]. However, the changes in the observed saturation moment were on the order of a few percent while the structural results were extracted from small changes in the ratio of two superlattice reflections (200 and 400), whose absolute intensities were small, such that changes may be easily over-/underestimated.

In this work, we aim to track irradiation-induced changes of the crystallographic order at the local level. To ensure full characterization of the structural order, we applied both local (TEM) as well as volume-integral probing (NMR) of He^{+}-irradiated Co$_2$MnSi thin films. The combination of magnetometry, nuclear magnetic resonance (NMR) and transmission electron microscopy (TEM) allows to get insights into the structure-property relationship, in particular linking both local and macroscopic properties. NMR probes the local environment of the investigated nuclei over the entire sample volume. It has already been shown that NMR is a potential method to resolve the evolution of structural order in functional materials[18,24–35]. By means of ^{59}Co NMR, we observe a

[1]IFW-Dresden, Institute for Solid State Research, Helmholtzstraße 20, 01069, Dresden, Germany. [2]Helmholtz-Zentrum Dresden-Rossendorf, Institute of Ion Beam Physics and Materials Research, Bautzner Landstrasse 400, 01328, Dresden, Germany. [3]National Institute of Materials Science, Tsukuba, Ibaraki, Japan. [4]Institute of Solid State and Materials Physics, TU Dresden, 01062, Dresden, Germany. Correspondence and requests for materials should be addressed to F.H. (email: f.hammerath@ifw-dresden.de)
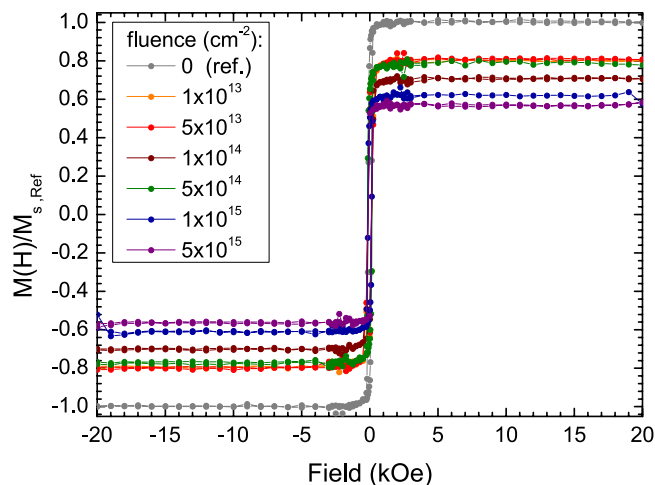
Figure 1. Magnetization of Co_2MnSi thin films at 300 K in fields up to 20 kOe for a non-irradiated reference sample (grey dots and lines) and the irradiated samples with He^+ ion fluences ranging from 10^{13} ions/cm² up to 5×10^{15} ions/cm². The data have been normalized to the data of the reference sample in saturation (20 kOe). The diamagnetic background from the substrate and the capping has been subtracted (See text for details).

degradation of the crystallographic order on a local scale from $L2_1$ to $A2$ order upon increasing He^+ ion fluence. We were able to deduce the amount of the respective $L2_1$- and $A2$-ordered phases for each applied fluence. We complement the NMR results by TEM which provides structural information of selected regions of the sample. The evolution of the structure is linked to the macroscopic magnetic properties showing a decrease of the saturated moment in response to the ion irradiation.

Methods

Co_2MnSi thin films of 40 nm thickness covered with a 5 nm thick Ta layer were deposited epitaxially on a (100) MgO substrate by magnetron sputtering and annealed at 500 °C. Samples of similar sizes (~7 × 7 mm²) have been cut and have been exposed to a 15 keV He^+ ion beam with fluences between 1×10^{13} and 5×10^{15} ions/cm². The ion beam was incident perpendicular to the film surface. This irradiation has been carried out at ambient temperature at the Ion Beam Center at the Helmholtz-Zentrum Dresden-Rossendorf. The displacements per atom (dpa) have been simulated using the binary collision approximation (Stopping and Range of Ions in Matter (SRIM) package)[36]. According to these simulations, 15 keV He^+ ions provide a nearly flat distribution of atomic displacements within the 40 nm thick Co_2MnSi film, while causing negligible intermixing with the capping layer and MgO substrate. The simulated dpa within the Co_2MnSi film varied from 0.001 to 0.56 for fluences of 1×10^{13} to 5×10^{15} ions/cm², respectively (see Supplementary Fig. 2 of supplementary material), leading to a statistical variation of the local ordering. NMR is an ideal tool to investigate such statistical variations.

The magnetization has been measured at 300 K using a superconducting quantum interference device (SQUID) from Quantum Design in the field range between −20 to 20 kOe. Please note, that the magnetization measured at 300 K does not significantly differ from the respective 5 K/0 K values due to the high Curie temperature of 985 K[37]. Zero-field (ZF) NMR measurements were performed at 5 K with an automated, coherent, phase-sensitive and frequency-tuned spin-echo spectrometer (NMR Service, Erfurt, Germany). A solid-echo sequence, consisting of two 90° pulses of 0.6 μs width, separated by 5 μs was used to observe the spin echo. This pulse sequence was repeated up to 2000 times to get a satisfying signal-to-noise ratio, while the repetition time between consecutive pulse sequences was kept long enough (100 ms) to prevent spin-lattice-relaxation effects on the measured spin-echo. The recorded spin-echo was integrated over the measured frequency range, which was swept in 1 MHz steps. The obtained NMR spectra were corrected for the enhancement factor as well as for the ν^2-dependence, resulting in relative intensities which are proportional to the number of nuclei with a given NMR resonance frequency.

High-resolution transmission electron microscopy (HRTEM) analysis was performed using an image C_s-corrected Titan 80–300 microscope (FEI) operated at an accelerating voltage of 300 kV. High-angle annular dark-field scanning transmission electron microscopy (HAADF-STEM) imaging and element mapping based on energy-dispersive X-ray spectroscopy (EDXS) were performed at 200 kV with a Talos F200X microscope (FEI) equipped with an X-FEG electron source and a Super-X EDXS detector system. Prior to TEM analysis, the specimen mounted in a double-tilt analytical holder was placed for 10 s into a Model 1020 Plasma Cleaner (Fischione) to remove contamination. Classical TEM specimen preparation based on sawing, grinding, polishing, dimpling, and final Ar ion milling was applied in the case of the sample irradiated with 5×10^{14} ions/cm².

Results

Magnetometry. The results from SQUID magnetometry performed at 300 K of the irradiated Co_2MnSi thin films are displayed in Fig. 1 together with the magnetization loop of a non-irradiated reference sample from the same batch. The diamagnetic background from the substrate and the Ta capping, which leads to a linear decrease (increase) at high (low) field values, has been subtracted. While the coercive field stays constant within error bars
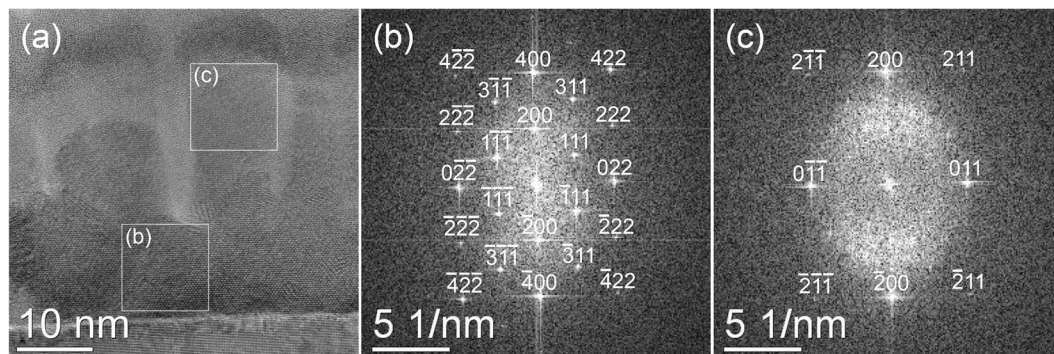
Figure 2. Cross-sectional HRTEM image (**a**) and corresponding fast Fourier transforms for the lower part (**b**) and upper part (**c**) of the sample irradiated with 5×10^{14} ions/cm^2, as obtained from the marked square areas.

(~125–160 Oe), the saturation magnetization decreases noticeably upon increasing the fluence. The biggest step occurs between the non-irradiated reference sample and the sample irradiated with the lowest fluence applied (10^{13} ions/cm^2, 20% reduction). The sample irradiated with the highest fluence (5×10^{15} ions/cm^2) exhibits a nearly halved saturation moment. Since magnetic properties of Heusler compounds are strongly linked to the underlying structural order, in the following, we will monitor the structural changes upon irradiation using TEM and NMR.

HRTEM. To study the evolution of the microstructure, HRTEM imaging of the non-irradiated reference and the sample irradiated with a fluence of 5×10^{14} ions/cm^2 were performed. In the non-irradiated state, fast Fourier transformation (FFT) analysis (see Supplementary Fig. 4 of supplementary material) points to the presence of the $L2_1$ structure, in good agreement to our NMR results (see following section). Regarding the sample irradiated with 5×10^{14} ions/cm^2, TEM analysis can differentiate between two sample regions. Evaluating the area close to the MgO substrate, i.e. the lower part of the Co$_2$MnSi film, the diffractograms obtained by FFT are indexed based on the $L2_1$ structure in [101] zone axis geometry [Fig. 2(b)], i.e. the same way as for the reference sample. In some parts of the upper Co$_2$MnSi film region, however, particular $L2_1$ reflections are strongly decreased in intensity or missing even completely, pointing to an increased disorder. These diffractograms can be better described with the $A2$ structure, also in [101] zone axis geometry [Fig. 2(c)]. These findings agree well with the NMR results, which found roughly a 50:50 distribution of $L2_1$ and $A2$ structure in this sample. While the NMR measurements cannot determine the location of these structure types within the Co$_2$MnSi layer, HRTEM analysis showed that $A2$ disorder is mostly present in the upper part of the film. Please note that light grey parts of Fig. 2(a) indicate the presence of oxide columns growing from the surface deep into the film (see supplementary material for details). These inclusions do not interfere with magnetization and NMR measurements, as discussed in detail in the Discussion section.

NMR. The inset of Fig. 3(a) shows the ^{59}Co NMR spectrum of the non-irradiated reference sample (annealed at 500 °C) in comparison to ^{59}Co NMR spectra of an $L2_1$-ordered polycrystalline bulk sample and a Co$_2$MnSi thin film, annealed at 550 °C[33]. Similar to these samples, the spectrum of the non-irradiated reference sample shows a maximum at around 147 MHz, characteristic for the Co$_2$MnSi phase, and a well-defined, reasonably small linewidth, representing a long-ranged, truly $L2_1$-ordered ^{59}Co environment (4 Mn and 4 Si atoms as nearest neighbors).

It exhibits a low frequency shoulder, stemming from a slight off-stoichiometry of excess Co atoms occupying Mn sites (Co^{Mn} antisites)[33]. The amount of Co^{Mn} antisites can be estimated by fitting the spectrum with Gaussian lines and comparing their relative areas to a binomial distribution function, resulting from a random atom model for the first shell environment of ^{59}Co[33,38–40]:

$$P(n, x) = \frac{N!}{(N-n)!n!}(1-x)^{N-n}x^n,$$

(1)

where $P(n, x)$ is the probability that n sites out of N sites are atoms of concentration x on those N sites. For the first Mn coordination shell (nearest neighboring Mn) of ^{59}Co, N is four and n runs from 0 to 4 in integer numbers. Figure 3 shows such a fit with three equidistant Gaussian lines of equal width (a) and a comparison between their relative areas with a probability function $P(n, x)$ for $x = 7.25\%$ (b) for the non-irradiated reference sample. The agreement between the fits and the distribution function is very high, which is further proven in a plot of their difference (c), not exceeding 2%.

Figure 4 shows the evolution of the corresponding ^{59}Co NMR spectra upon the irradiation with He$^+$ ions for all applied fluences. Already for moderate fluences (10^{13}–10^{14} cm^{-2}), the spectrum broadens slightly, compared to the non-irradiated sample, reflecting an increasing structural disorder. For higher fluences (5×10^{14}–10^{15} cm^{-2}), the broadening gets even more pronounced and the peak frequency shifts to lower values. The spectrum of the sample irradiated with the highest fluence (5×10^{15} cm^{-2}) is completely smeared out over the whole measured frequency range and no distinct peak can be identified. Such a broad NMR resonance line is typical for a completely
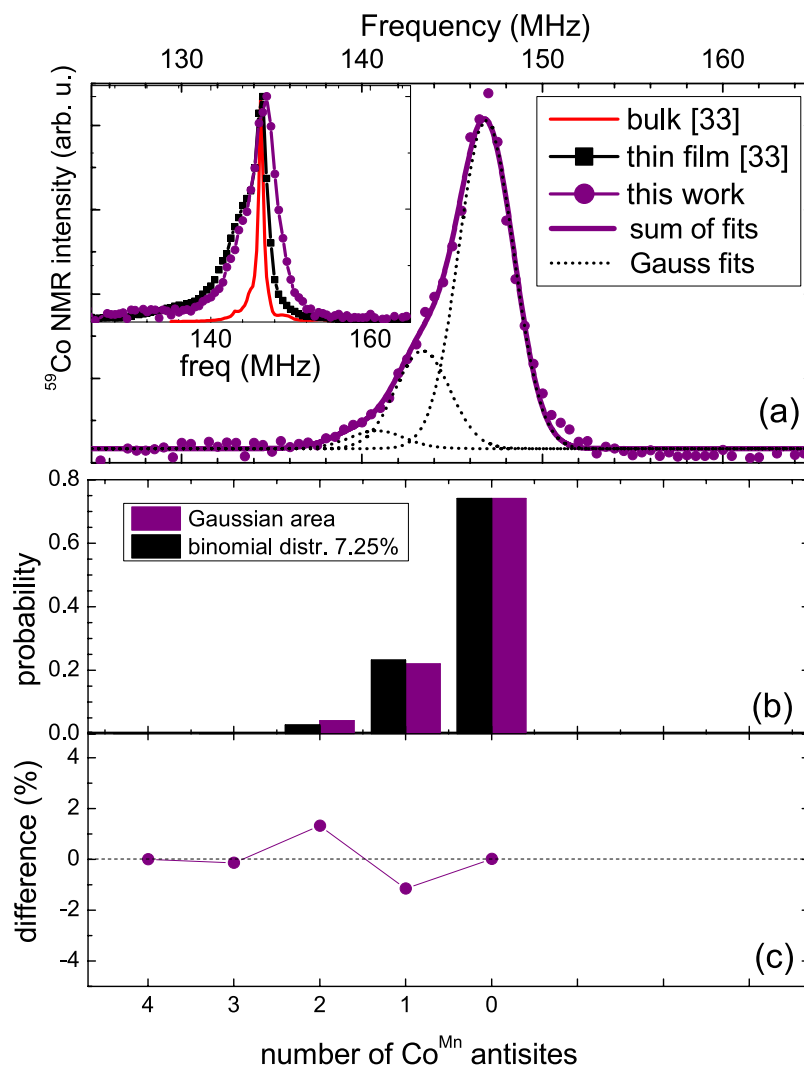
Figure 3. (**a**) ^{59}Co NMR spectra at 5 K for the non-irradiated reference sample (purple dots). Dotted lines are fits with Gaussian lines, representing the off-stoichiometry. The thick purple line is the sum of these Gaussian lines. The inset shows a comparison of the ^{59}Co NMR spectra of the reference sample (purple dots and line), to a Co$_2$MnSi thin film annealed at 550 °C (black squares and line) and a bulk polycrystalline Co$_2$MnSi sample (red line)[33]. (**b**) Probability $P(n, x)$ of the binomial distribution function for $x = 7.25\%$ (black columns) in comparison to the relative areas of the Gaussian fits to the spectrum (purple columns). (**c**) Difference between the relative areas of the Gaussian lines and the binomial probability.

disordered $A2$ structure type, where, due to a complete intermixing of all atomic sites, a plethora of different first shell environments exists for the ^{59}Co nuclei, leading to a distribution of many different hyperfine fields[28,41] (see Supplementary Fig. 1 of supplementary material for the $L2_1$ and $A2$ structure types, their corresponding first shell environments and expected NMR spectra).

Figure 5 (A–E) show Gaussian fits to the spectra of the irradiated samples. Three dotted lines indicate the off-stoichiometric $L2_1$ phase, similar as already discussed for the non-irradiated reference sample [Fig. 3(a)]. An additional broad Gaussian line (filled light grey line) represents the emerging $A2$ structure formation. This $A2$ contribution evolves already for the smallest fluence used. Its percentage increases upon increasing the fluence [see Fig. 5(F)], until reaching 100% for the sample irradiated with the highest fluence (5×10^{15} cm^{-2}, see Fig. 4). The full width at half maximum (FWHM) of the $L2_1$ peaks also increases [see Figs 4 and 5(F)]. Due to the increased linewidths, only two Gaussians can be fitted for the $L2_1$ order in the last spectrum [Fig. 5(E)]. The spectrum for the highest fluence (5×10^{15} cm^{-2}) is omitted in this plot, since its broad NMR line, ranging over the whole measured frequency range, represents a 100% disordered $A2$ structure type.

Our NMR measurements show that for the considered range of He$^+$ fluences, ion irradiation leads to an increase of structural disorder at the local scale, going along with a strong impact on the macroscopic magnetic properties, even for the lowest fluences applied. We observe a direct crossover from the highly-ordered $L2_1$ to the completely disordered $A2$ structure upon increasing the He$^+$ fluence.
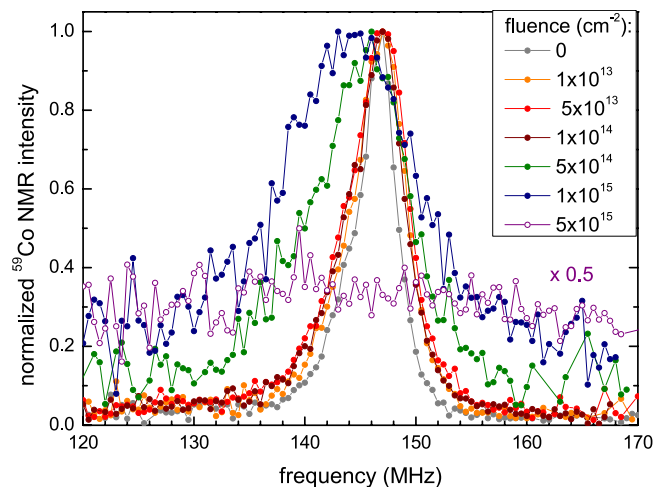
Figure 4. Normalized ^{59}Co NMR spectra of the irradiated films in comparison to the non-irradiated reference sample.
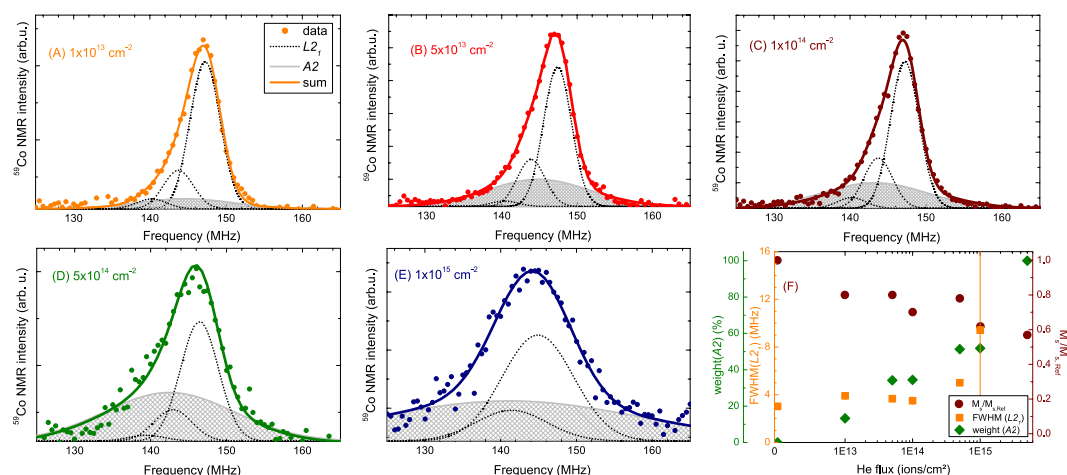

Figure 5. (**A–E**) ^{59}Co NMR spectra at 5 K for irradiated samples starting with the lowest flux of 1×10^{13} ions/cm^2 up to 1×10^{15} ions/cm^2. The corresponding fluence is written in the graphs. Lines are fits with Gaussian lines to the spectra. Dotted black lines denote the Gaussians representing the off-stoichiometric $L2_1$ ordered regions of the samples, while the filled light grey line corresponds to the *A2*-ordered regions of the sample. The thick line in the color of the respective data dots is the sum of all Gaussian lines. (**F**) Irradiation-dependent weight of the A2 structure type (dark green diamonds), FWHM of the $L2_1$ phase (orange squares), and the corresponding change in the saturation moment (dark red dots).

Discussion

Several conclusions can be drawn from the NMR data:

The NMR spectra of all samples show a low-frequency shoulder, which can be fitted assuming three Gaussian lines, whose intensity distributions reflect a slight off-stoi-chiometry of 7.25% excess Co on Mn sites. This kind of off-stoichiometry of an otherwise highly-ordered $L2_1$ Heusler structure has been frequently observed in thin films and is typical for stoichiometric sputter targets. It arises from differences in the sputtering rates of individual elements[8,30,33,40,42]. For the investigated samples, the antisite concentration x has been found to be the same throughout the whole irradiation series (see supplementary material).

The $L2_1$ lines broaden with increasing ion fluence and an additional, very broad A2 line evolves. These observations imply changes in the local structure of the ^{59}Co atoms on different coordination shells: (i) The probability to have a random distribution of all atoms in higher coordination shells increases. This disorder manifests mainly in the increasing FWHM of the $L2_1$ Gaussian lines (dark grey lines in Fig. 5) [(see Fig. 5(F)]. (ii) At the same time, the probability to change also the first coordination shell, which for the non-irradiated sample consists of 4 Mn and 4 Si atoms, increases with increasing fluence. Since within the A2 type (dis)order the total number of different possible atomic configurations in all atomic coordination shells is very large, as is the number of their internal fields, these structural changes lead to the observed additional broad NMR line. For the highest fluences, the majority of Co atoms has a local environment different to those from the non-irradiated sample.

Reference	E (keV)	fluence (ions/cm^2)	structure of starting material	structural evolution
this work	15	10^{13}–10^{15}	$L2_1$	decrease of structural order ($A2$)
Gaier *et al.*[23]	30	10^{14}–10^{16}	$B2 + A2$	increase of structural order ($B2$)
Abdallah *et al.*[43]	150	10^{15}–10^{16}	$L2_1 + B2$ grains	decrease of structural order ($B2$ and $D0_3$)

Table 1. Overview of studies on He$^+$-irradiated Co$_2$MnSi thin films, their corresponding experimental conditions and the resulting change of structural properties.

Regarding the type of emerging disorder upon ion irradiation, in principle other structure types such as $B2$ or DO_3 are imaginable. In fact, a similar study on 40 nm thin films of Co$_2$MnSi (originally $L2_1$-ordered with some small grains of $B2$ order) irradiated with He$^+$ ions of much higher energy (150 keV, 10^{15}–10^{16} ions/cm^2) reported an increase of $B2$ and DO_3 disorder upon increasing fluence by means of XRD and HAADF-STEM[43]. However, our NMR spectra do not show any sign of these structure types. For $B2$, with an intermixing of Mn and Si sites, the NMR spectrum should show additional, well-separated peaks with a fixed spacing on both sides of the central peak[28,41]. In the case of DO_3 order (Co-Mn intermixing), peaks with different intensities and spacings on both sides of the central peak would be expected, stemming from the 1st and 2nd coordination shells[2]. The broad additional line in the NMR spectrum of our samples, which evolves upon irradiation, indicates emerging $A2$ disorder, in excellent agreement with the HRTEM results.

With this study, there are now three different reports on the impact of He$^+$ irradiation on Co$_2$MnSi thin films (which are summarized in Table 1): Gaier *et al.* reported an improvement of structural and magnetic properties upon the irradiation with 30 keV He$^+$ ions for a certain range of fluences (around 10^{14} ions/cm^2)[23]; a more recent study showed an increase of $B2$ and DO_3 disorder and a reduced magnetization by using 150 keV He$^+$ ions of 10^{15} to 10^{16} ions/cm^2[43,44]; while the present work reports a direct crossover from highly-ordered $L2_1$ to completely disordered $A2$ structure (15 keV, 10^{13}–10^{15} ions/cm^2), without inducing other structure types. SRIM calculations (not shown) showed that there is only a slight difference in the average Co displacement upon changing the ion beam energy from 15 to 30 keV He$^+$ ions. The irradiation with 150 keV He$^+$ ions is supposed to lead to bigger differences from local heating due to the larger deposited energy. Apart from the different energies, an explanation for the observed variations might be the different starting conditions. Gaier *et al.* used $B2$-ordered films with a certain admixture of $A2$-disordered regions as starting material. They conclude that the increase of $B2$ order originates from initially $B2$-ordered regions, due to Co - Mn and Co - Si exchanges caused by mobile vacancies introduced by the irradiation. Similarly, the $L2_1$-ordered films from Abdallah *et al.* already contained some very small grains of $B2$ order, which might have favored a (in this case degrading) $B2$ transformation starting from these initial nucleation sites. The starting material of the present study is highly $L2_1$-ordered. The displacement of atoms caused by the incident ion beam produces vacancies, which will stochastically recombine with thermally diffusing atoms resulting in disorder. Since there are no $B2$ nucleation sites, we expect an arbitrary intermixing of all atoms at all sites, leading to the completely disordered $A2$ structure, as observed here.

It should also be noted that the reported improvement of $B2$ structure and magnetic properties in ref.[23] is limited to a certain range of fluences (1–5×10^{14} ions/cm^2) for which only a very subtle increase of structural order and saturation moment were observed. For higher fluences also this study found a substantial degradation of structural and magnetic properties.

One of the advantages of the NMR technique is that it allows to probe the local environments of all Co atoms in the film sample in one measurement. (Assuming a relative permeability of 600 (Co) and taking the reported resistivity values of Co$_2$MnSi at 5 K, which range from 4–40 $\mu\Omega$ cm[11,37,45], the skin depth of the penetrating microwave amounts to 400–1000 nm[46], which is far more than the film thickness). While we are probing the full volume of the film without any losses due to film thickness, the NMR method does not reveal from which position in the samples a certain NMR signal is excited, e.g., from Co atoms at the top or at the bottom of the film. Hence, we complemented the NMR results with TEM which can provide spatially resolved information about the local structure at a specific sample position.

According to our HRTEM results, there is a depth-dependent structural order in the irradiated samples: regions next to the surface are mainly $A2$-ordered, while regions next to the substrate still retain the original $L2_1$ structure. In comparison to the SRIM simulations, which showed a rather flat distribution of atomic displacements within the Co$_2$MnSi film (see Supplementary Fig. 2 of supplementary material), this is rather surprising. One may consider this observation to be triggered by the presence of oxide columns growing from the surface deep into the film (down to about 20 nm deep into the film; see Supplementary Fig. 5 of supplementary material and discussion in following paragraph). Here, oxygen may nucleate the vacancies leading to a higher probability for atomic displacements in their vicinity.

Our results underline that structure analysis by NMR, which allows quantitative determination of phase fractions on an integral scale, and by TEM, which enables imaging down to the atomic scale, complement each other very well. A similar combination of NMR and TEM was already successfully used to study the chemical composition of multi-element nanostructures[35].

We now turn to the relation between (local) structure and macroscopic magnetic properties. Note that the absolute value of the saturated moment of our non-irradiated reference sample (2.7 μ_B/f.u. at 300 K, which translates to 2.8 μ_B at 5 K[37]) is lower than the theoretically expected and experimentally verified value of 5 μ_B/f.u.[12,45]. Two issues contribute to the lower absolute value of the saturated moment: (i) Reduced saturated moments have also been reported for other $L2_1$-ordered Heusler thin films sputtered from stoichiometric targets, e.g., Co$_2$FeSi (4.5–5 μ_B instead of 6 μ_B)[40,47,48]. This difference most likely results from the mentioned off-stoichiometry due to

selective sputtering. A polycrystalline bulk sample intentionally prepared with a corresponding off-stoichiometry, namely $Co_{2.1}Mn_{0.9}Si$, indeed showed a reduced saturation moment of 4.6 μ_B/f.u. (see Supplementary Fig. 3 of supplementary material). Other theoretical and experimental work on Co_2MnSi found comparable effects of Co antisites on the corresponding saturation moments (4.75–4.9 μ_B, respectively)[14,16,17]. However, the deviation from the expected value for our reference sample is too big (nearly 50%) to be solely explained by a slight Co excess. (ii) In fact, our samples contain considerable amounts of oxide phases (see detailed discussion in supplementary material). In the case of magnetization data, these oxide phases do not contribute to the ferromagnetic signal, but lead to an overestimation of the intrinsic Co_2MnSi mass when calculating the magnetization and, thus, to a reduced absolute saturation moment. Importantly, the presence of these oxides does not interfere with the NMR analysis. Measurements of the variations of the local ^{59}Co environment have been made from the same initial state on all samples, namely from the remaining non-oxidized parts of the samples, which gave rise to the ferro-magnetic SQUID signals. These are well-characterized Co_2MnSi regions, as proven by HRTEM (Fig. 2) and NMR analysis [see inset of Fig. 3(a)]. Both the off-stoichiometry and the overestimation of the intrinsic Co_2MnSi mass due to the presence of oxides are expected to be present and on the same order of magnitude in all samples before the irradiation process. Our discussion of the changes in the structure-property relationship of the Co_2MnSi thin films upon the irradiation with He^+ ions is therefore straightforward and not affected by the presence of oxide inclusions or slight off-stoichiometry.

Finally, we see a clear trend of decreasing moment with increasing ion fluence mimicking the inverse trend of increasing disorder with increasing fluence. These observations are in line with previous studies showing a strong dependence of the magnetic moment on the crystal structure[47,49,50]. Even for moderate fluences (around 10^{14} ions/cm^2), where, based on XMCD measurements, an increasing saturation moment has been reported for Co_2MnSi thin films irradiated with He^+ ions of similar energy (30 keV)[23], we see a clear trend towards lower saturation moments and a substantial fraction of $A2$ structure. Hence, ion-irradiation can subtly vary the local environment, thereby revealing structure-property relationships in Heusler compounds.

Conclusion

Combined magnetization, NMR, and TEM measurements of Co_2MnSi thin films under the impact of He^+ irradiation showed that, even for the lowest fluences applied, the moment in saturation decreases, going along with an increased structural disorder. The disorder manifests itself in a transition from a highly $L2_1$-ordered to a completely disordered $A2$ structure in a sample irradiated with the highest fluence applied (5×10^{15} He^+ ions/cm^2). The direct transition from $L2_1$ to $A2$ has been revealed by NMR measurements, which could deduce the amounts of $L2_1$- and $A2$-ordered phases in each of the thin films. The NMR measurements also revealed a slight off-stoichiometry of 7.25% Co excess, which is constant throughout the films, indicating that it originates from their preparation process. Complementary HRTEM analyses added local information of the distribution of $L2_1$ and $A2$ phases in the sample, revealing that the $A2$ disorder is mainly located at the upper part of the films in vicinity to the film surface.

References

 1. de Groot, R. A., Mueller, F. M., Engen, P. G. V. & Buschow, K. H. J. New class of materials: Half-metallic ferromagnets. *Phys. Rev. Lett.* **50**, 2024–2027 (1983).
 2. Kandpal, H. C., Fecher, G. H. & Felser, C. Calculated electronic and magnetic properties of the half-metallic, transition metal based Heusler compounds. *J. Phys. D: Appl. Phys.* **40**, 1507 (2007).
 3. Wurmehl, S. *et al.* Investigation of Co_2FeSi: The Heusler compound with highest Curie temperature and magnetic moment. *Appl. Phys. Lett.* **88**, 032503 (2006).
 4. Yang, F. J. *et al.* Anisotropic magnetoresistance in Co_2(Fe, Mn)Si Heusler epitaxial films: A fingerprint of half-metallicity. *Phys. Rev. B* **86**, 020409 (2012).
 5. Sakuraba, Y. *et al.* Quantitative analysis of anisotropic magnetoresistance in Co_2MnZ and Co_2FeZ epitaxial thin films: A facile way to investigate spin-polarization in half-metallic Heusler compounds. *Appl. Phys. Lett.* **104**, 172407 (2014).
 6. Sakuraba, Y., Ueda, M., Bosu, S., Saito, K. & Takanashi, K. CPP-GMR study of half-metallic full-Heusler compound Co_2(Fe, Mn)Si. *J. Magn. Soc. Jpn.* **38**, 45–49 (2014).
 7. Schmalhorst, J. *et al.* Interface structure and magnetism of magnetic tunnel junctions with a Co_2MnSi electrode. *Phys. Rev. B* **70**, 024426 (2004).
 8. Sakuraba, Y. *et al.* Direct observation of half-metallic energy gap in Co_2MnSi by tunneling conductance spectroscopy. *Appl. Phys. Lett.* **89**, 052508 (2006).
 9. Ishikawa, T. *et al.* Spin-dependent tunneling characteristics of fully epitaxial magnetic tunneling junctions with a full-Heusler alloy Co_2MnSi thin film and a MgO tunnel barrier. *Appl. Phys. Lett.* **89**, 192505 (2006).
10. Sakuraba, Y. *et al.* Giant tunneling magnetoresistance in Co_2MnSi/Al–O/Co_2MnSi magnetic tunnel junctions. *Appl. Phys. Lett.* **88**, 192508 (2006).
11. Sakuraba, Y. *et al.* Mechanism of large magnetoresistance in Co_2MnSi/Ag/Co_2MnSi devices with current perpendicular to the plane. *Phys. Rev. B* **82**, 094444 (2010).
12. Brown, P. J., Neumann, K. U., Webster, P. J. & Ziebeck, K. R. A. The magnetization distributions in some Heusler alloys proposed as half-metallic ferromagnets. *J. Physics: Condens. Matter* **12**, 1827 (2000).
13. Picozzi, S., Continenza, A. & Freeman, A. J. Co_2MnX (X = Si, Ge, Sn) Heusler compounds: An ab initio study of their structural, electronic, and magnetic properties at zero and elevated pressure. *Phys. Rev. B* **66**, 094421 (2002).
14. Picozzi, S., Continenza, A. & Freeman, A. J. Role of structural defects on the half-metallic character of Co_2MnGe and Co_2MnSi Heusler alloys. *Phys. Rev. B* **69**, 094423 (2004).
15. Miura, Y., Nagao, K. & Shirai, M. Atomic disorder effects on half-metallicity of the full-Heusler alloys $Co_2Cr_{1-x}Fe_x$)Al: A first-principles study. *Phys. Rev. B* **69**, 144413 (2004).
16. Raphael, M. P. *et al.* Presence of antisite disorder and its characterization in the predicted half-metal Co_2MnSi. *Phys. Rev. B* **66**, 104429 (2002).
17. Kogachi, M., Fujiwara, T. & Kikuchi, S. Atomic disorder and magnetic property in Co-based Heusler alloys Co_2MnZ (Z = Si, Ge, Sn). *J. Alloy. Compd.* **475**, 723–729 (2009).
18. Wurmehl, S. *Structural Order in Heusler Compounds. In: Heusler alloys - properties, growth, applications.* (Eds Felser, C. & Hirohata, A.) and references therein (Springer, 2016).

19. Fassbender, J., Ravelosona, D. & Samson, Y. Tailoring magnetism by light-ion irradiation. *J. Phys. D: Appl. Phys.* **37**, R179 (2004).
20. Bali, R. *et al*. Printing nearly-discrete magnetic patterns using chemical disorder induced ferromagnetism. *Nano Lett.* **14**, 435–441 (2014).
21. Heidarian, A. *et al*. Tuning the antiferromagnetic to ferromagnetic phase transition in FeRh thin films by means of low-energy/low fluence ion irradiation. *Nucl. Instruments Methods Phys. Res. Sect. B: Beam Interactions with Mater. Atoms* **358**, 251–254 (2015).
22. Ravelosona, D., Chappert, C., Mathet, V. & Bernas, H. Chemical order induced by ion irradiation in FePt (001) films. *Appl. Phys. Lett.* **76**, 236–238 (2000).
23. Gaier, O. *et al*. Improvement of structural, electronic, and magnetic properties of Co_2MnSi thin films by He^+ irradiation. *Appl. Phys. Lett.* **94**, 152508 (2009).
24. Niculescu, V. A. *et al*. Relating structural, magnetic-moment, and hyperfine-field behavior to a local-environment model in $Fe_{3-x}Co_xSi$. *Phys. Rev. B* **19**, 452 (1979).
25. Endo, K., Ooiwa, K. & Shinogi, A. Structural phase transitions and magnetism in $Ni_2Mn_{1-x}V_xGa$ and $(Co_{1-y}Ni_y)_2NbSn$. *J. Magn. Magn. Mat.* **104-107**, 2013–214 (1992).
26. Jay, J. P., Wójcik, M. & Panissod, P. Hyperfine field and ordering in bcc CoFe bulk alloys studied by ^{59}Co NMR and monte-carlo simulation. *Zeitschrift für Physik B Condens. Matter* **101**, 471–486 (1996).
27. Panissod, P. Structural and magnetic investigations by NMR. application to magnetic multilayers. In Baryakhtar, V. G., Wigen, P. E. & Lesnik, N. A. (eds) *NATO ASI series High Tech*, vol. 48, 225 (Kluwer Academic, Dordrecht, 1997).
28. Inomata, K. *et al*. Structural and magnetic properties and tunnel magnetoresistance for $Co_2(Cr, Fe)Al$ and Co_2FeSi full-Heusler alloys. *J. Phys. D: Appl. Phys.* **39**, 816 (2006).
29. Ksenofontov, V. *et al*. Structure and properties of CoMnSb in the context of half-metallic ferromagnetism. *Phys. Rev. B* **74**, 134426 (2006).
30. Inomata, K., Wojcik, M., Jedryka, E., Ikeda, N. & Tezuka, N. Site disorder in $Co_2Fe(Al, Si)$ Heusler alloys and its influence on junction tunnel magnetoresistance. *Phys. Rev. B* **77**, 214425 (2008).
31. Wurmehl, S. *et al*. Local formation of a Heusler structure in CoFe-Al alloys. *Appl. Phys. Lett.* **98**, 12506 (2011).
32. Wójcik, M., Jedryka, E., Sukegawa, H., Nakatani, T. & Inomata, K. ^{59}Co NMR experiment as a probe of electron doping in $Co_2FeAl_{1-x}Si_x$ Heusler alloys. *Phys. Rev. B* **85**, 100401 (2012).
33. Rodan, S. *et al*. Nuclear magnetic resonance reveals structural evolution upon annealing in epitaxial Co_2MnSi Heusler films. *Appl. Phys. Lett.* **102**, 242404 (2013).
34. Wurmehl, S. & Kohlhepp, J. T. NMR spectroscopy on Heusler thin films - a review. *Spin* **4**, 1440019 (2014).
35. Gellesch, M. *et al*. Compositional analysis of multi-element magnetic nanoparticles with a combined NMR and TEM approach. *J. Nanoparticle Res.* **19**, 307 (2017).
36. Ziegler, J. F., Ziegler, M. & Biersack, J. SRIM: The stopping and range of ions in matter (2010). *Nucl. Instruments Methods Phys. Res. Sect. B: Beam Interactions with Mater. Atoms* **268**, 1818–1823 (2010).
37. Ritchie, L. *et al*. Magnetic, structural, and transport properties of the Heusler alloys Co_2MnSi and NiMnSb. *Phys. Rev. B* **68**, 104430 (2003).
38. Wurmehl, S. *et al*. Probing the random distribution of half-metallic $Co_2Mn_{1-x}Fe_xSi$ Heusler alloys. *Appl. Phys. Lett.* **91**, 052506 (2007).
39. Schaf, J., Campbell, I., Dang, K. L., Veillet, P. & Hamzik, A. NMR and magnetization study of the mixed systems $(Pd_{1-x}Cu_x)_2MnIn$ and $(Pd_{1-x}Ni_x)_2MnIn$. *J. Magn. Magn. Mater.* **36**, 310–318 (1983).
40. Wurmehl, S. *et al*. Off-stoichiometry in Co_2FeSi thin films sputtered from stoichiometric targets revealed by nuclear magnetic resonance. *J. Phys. D: Appl. Phys.* **42**, 084017 (2009).
41. Wurmehl, S., Kohlhepp, J. T., Swagten, H. J. M. & Koopmans, B. Hyperfine field distribution in the Heusler compound Co_2FeAl probed by ^{59}Co nuclear magnetic resonance. *J. Phys. D: Appl. Phys.* **41**, 115007 (2008).
42. Oogane, M. *et al*. Large tunnel magnetoresistance in magnetic tunnel junctions using Co_2MnX (X = Al, Si) Heusler alloys. *J. Phys. D: Appl. Phys.* **39**, 834 (2006).
43. Abdallah, I. *et al*. Structural and magnetic properties of He^+ irradiated Co_2MnSi Heusler alloys. *Mater. Res. Express* **3**, 046101 (2016).
44. Abdallah, I. *et al*. Evolution of magnetic properties and damping coefficient of Co_2MnSi Heusler alloy with Mn/Si and Co/Mn atomic disorder. *J. Phys. D: Appl. Phys.* **50**, 035003 (2017).
45. Raphael, M. P. *et al*. Magnetic, structural, and transport properties of thin film and single crystal Co_2MnSi. *Appl. Phys. Lett.* **79**, 4396–4398 (2001).
46. Abragam, A. Principles of Nuclear Magnetism (Oxford University Press, New York, 1961).
47. Tezuka, N., Okamura, S., Miyazaki, A., Kikuchi, M. & Inomata, K. Structural dependence of the tunnel magnetoresistance for magnetic tunnel junctions with a full-Heusler $Co_2Fe(Al, Si)$ electrode. *J. Appl. Phys.* **99**, 08T314 (2006).
48. Schneider, H. *et al*. Epitaxial film growth and magnetic properties of Co_2FeSi. *Phys. Rev. B* **74**, 174426 (2006).
49. Kudryavtsev, Y. V. *et al*. Effect of structural disorder on some physical properties of the Cu_2MnAl Heusler alloy films. *J. Appl. Phys.* **97**, 113903 (2005).
50. Wurmehl, S. *et al*. Electronic structure and spectroscopy of the quaternary Heusler alloy $Co_2Cr_{1-x}Fe_xAl$. *J. Phys. D: Appl. Phys.* **39**, 803 (2006).

Acknowledgements

Author Contributions

F.H. conducted the NMR and magnetometry measurements and analysed the data; F.H., R. Bali, R.H. and S.W. wrote the manuscript; R. Bali performed the SRIM calculations; R. Bali, K.P. and R. Böttger conducted the ion irradiation; R.H. conducted the HRTEM and HAADF-STEM experiments and analysed the corresponding data; M.R.D.B. assisted the NMR and magnetometry measurements; S.R. synthesized and characterized the off-stoichiometric bulk sample; Y.S. provided the films samples; S.W., F.H. and R. Bali conceived the project. All authors reviewed the manuscript.

Additional Information

Competing Interests: The authors declare no competing interests.

Publisher's note: Springer Nature remains neutral with regard to jurisdictional claims in published maps and institutional affiliations.